Etching and Aging Effects in Nanosize Au Clusters Investigated Using High-Resolution Size-Exclusion Chromatography

Jess P. Wilcoxon* and Paula Provencio

Nanostructures and Advanced Materials Chemistry, Department 1122, Sandia National Laboratories, Albuquerque, New Mexico 87185-1421

Received: November 27, 2002; In Final Form: September 12, 2003

We report experiments using high-resolution size exclusion chromatography (HRSEC), dynamic light scattering, and transmission electron microscopy to investigate the effects of aging of Au nanoclusters in the presence of surfactant ligands. We first describe our observations of the role of thiols as etchants to produce clusters in a micelle-free synthesis by reduction of a metal−organic precursor. Clusters with large abundances are identified using HRSEC, and their sizes and optical properties are reported. The smallest, $D_c \sim 1$ nm molecular sized Au clusters, with approximately 1 closed atomic shell, N ∼ 13 atoms, have nonclassical features in their room temperature absorbance spectra. The other dominant sub-populations also correspond closely to closed-shell structural stabilities. We show that, contrary to the expectation that aging in solution will always broaden the size dispersion and increase the average size (Ostwald ripening), a narrowing of the size dispersion and change in average size can occur with time under ambient conditions. In the presence of various chain length alkanethiols, an etching and size decrease usually occurs; in the case of weakly bound alkylated poly(ethylene oxide) surfactants, an increase in size with time is observed.

1. Introduction

One of the earliest and best known examples of cluster growth from atomic precursors in solution was the synthesis by Schmid of Au(N=55) clusters by diborane reduction of gold tri-phenyl phosphine chloride in benzene or methylene chloride.[1] Fifty-five atoms of a metal corresponds to the closing of the second atomic shell of a Au($N = 13$) cluster core with 42 Au atoms with a dozen tri-phenyl phosphine molecules weakly ligated to the faces of the inorganic core. For a given cluster diameter, the number of atoms in an unpassivated or naked spherical metal nanocluster with cubic close-packing of atoms (fcc or hcp type) is much larger than for ligated metal clusters grown in solution. For example, bare Au clusters with a spherical, close-packed geometry and $N \sim 120$ atoms have a diameter 1.5−1.6 nm which corresponds in core size to Schmid's cubicosahedral Au core which has only $N = 55$ atoms. So, the role of the ligand used to sterically stabilize inorganic nanoclusters in a solvent is critical in determining the stable structure and size of a given nanocluster.

Due to the lack of stability of Au($N = 55$) clusters in the high-vacuum conditions required for TEM, it has not been possible to demonstrate the presence of discrete clusters with cross-sectional sizes of only 1.5 nm, made by the Schmid approach. Instead, larger aggregates were observed. In general, in somewhat polydisperse samples of nanoclusters it is very challenging to objectively determine the size and relative abundance of each cluster sub-population. This means that new analytic approaches to nanocluster size characterization as a function of synthetic method, ligand type, and sample age are required.

Recently, using high-resolution size-exclusion chromatography, we have demonstrated that special sizes occur in a wide range of inverse micelle growth experiments.[2] This preference for special sizes in solution growth processes is found in both simple metals and semiconductor nanocrystals.[3] The only requirement seems to be that the size be less than ∼3−4 nm, and that diffusion and intercluster material exchange may occur over time.

When clusters are grown by the inverse micelle process in organic liquid,[4−7] in the presence of alkanethiol molecules, certain sizes are especially abundant.[8] Using MALDI-TOF mass spectroscopy to analyze the cluster mass distribution, the Whetten group has demonstrated the ubiquitous presence of a 29 kDa Au cluster compound,[9] formed in large abundance when sufficient numbers of alkanethiols are present during the cluster growth process. In the absence of thiol, a much broader size distribution is observed. Recently, they have extended this controlled etching process to polydisperse samples by heating the sample for long periods in pure alkanethiol.[10] A similar digestive ripening process for clusters synthesized in inverse micelles has been described by Lin et al.[11] Certain special-sized clusters occurred in both reports.

In this paper, we describe the effect of ligand etching processes and sample aging on the size distribution of Au colloids, formed by two approaches. The first uses a modified, surfactant-free method of Schmid, while the second uses the inverse micelle growth approach.[6] To observe the changes in average size and size dispersion with age and surfactant we use high-resolution size-exclusion chromatrography to size separate and determine the optical properties of the clusters.[12,13] Our size analysis method is both faster and more precise (1−2 Å resolution) than TEM analysis and less subject to experimental artifacts associated with exposing nanosize clusters stabilized by organic ligands to a high vacuum and intense electron beams (e.g., size-segregation, cluster melting, ligand desorption, and cluster coalescence).

* Corresponding author. E-mail: jpwilco@sandia.gov.

10.1021/jp027575y CCC: $25.00
Published on Web 10/31/2003

In the first part of the paper we describe HRSEC size and optical analysis of clusters synthesized using the Schmid process modified by the use of organic metal hydride reducing agents instead of diborane. In this process, alkanethiols are added post-reduction and act as etchants producing certain preferred sizes. In the second part, we give examples of the size evolution of Au clusters with age for both cationic and nonionic inverse micelle synthesis. We demonstrate the role of dilute amounts of alkanethiols added post-reduction as chemical etchants which produce smaller, more monodisperse clusters from larger ones.

2. Experimental Section

A. Size-Exclusion Chromatography. A Water's Corporation delta-prep commercial high-pressure liquid chromatography equipped with automated injector (model 717), and two detectors, a photodiode array absorbance spectrometer (model 996), and differential refractive index detector (model 410) were used to detect elution of the nanoclusters and nonabsorbing organic chemicals, respectively. A high-resolution Polymer's laboratory model PL500 or PL1000 cross-linked polystyrene column filled with 5 μm microgel particles and having 500 or 1000 Å pores was used to separate the nanoparticles. The columns are a high-resolution, "semi-prep" type, with dimensions of 7.6 mm × 300 mm, filled with 5 μm gel particles. The inherent instrumental line width for pure solvents (full width, half-height) is ∼0.25 min with these columns which allows nearly baseline resolution of cluster populations differing by only ∼1 nm. The mobile phase was HPLC grade toluene with dodecanethiol at 0.01 M added to prevent cluster adhesion to the column and achieve a symmetrical elution peak shape. A constant flow rate of 1.0 mL/min was used in all the experiments and the total back pressure due to the solvent filter, guard column, column, and the two in-line detectors was ∼700 psi at ambient temperatures.

The relationship between retention time and hydrodynamic diameter with size standards has been described previously in two papers, where it was demonstrated that in the absence of specific chemical interactions between the cluster and the column, the time, t, required for elution is related to the hydrodynamic diameter, D_h, of the cluster by $\log D_h \sim t$. Using this calibration approach based upon nanocluster, polystyrene, and alkane standards for a given column, we obtain the cluster hydrodynamic diameter, D_h (inorganic core + total organic shell thickness), from the elution time, t, where $\log D_h \sim t$ for pure SEC.[14] For example, for a model PL1000 column with a guard column, an excellent fit of $D_h(\text{nm}) = 608 \times \exp(-0.62525 \times t(\text{min}))$ is obtained where D_h(nm) is obtained independently (or calculated in the case of alkanes) from dynamic light scattering for the larger clusters and polymer standards.[2] We independently confirm this relation between retention time and D_h on filtered PS and Au cluster/thiolate systems having $D_h > 5$ nm.

An in-line filter and short "guard" column of the same column material is used to prevent retention time changes with age and/or injection of aggregated samples. With such a system we can reproduce the retention time or hydrodynamic size of high-quality, stable nanocluster samples to within the instrument resolution of 0.01−0.02 min over periods greater than 1 year. This corresponds to a size resolution (see spectral homogeneity discussion below) of ∼1−2 Å.

B. Transmission Electron Microscopy (TEM). Bright-field TEM was done on a JEOL EX at 120 kV with a point-to-point resolution of approximately 9 Å. Magnifications of 50K× or 100K× were used to obtain diffraction contrast images. A JEOL model 2010 was used to obtain high-resolution lattice fringe images at magnifications of 600K× or 800K×. An ∼2 μL drop of a ∼0.01 M (atomic molarity) cluster solution in toluene is applied to the holey carbon grid which rests on absorbent filter paper which rapidly wicks away the solvent, allowing the clusters to be well dispersed on the grid. With slower drying cluster pile-up, formation of supracrystals is favored, as we have demonstrated in recent publications where further details of our TEM procedures were given.[15,16]

C. Dynamic Light Scattering (DLS). The intensity autocorrelation function of the scattered light from dilute solutions of nanoclusters was determined using a Brookhaven Instruments model 9000 autocorrelator. A He−Ne laser operating at 632.8 nm and an intensity of ∼13 mW was used as a scattering excitation source, and the nanocluster samples were contained in 2 mm path length cuvettes to maximize the extracted light. The quasi-elastically scattered light was collected perpendicular to the incident beam by a Thorn-EMI S20 type photomultiplier tube. Our measurements were restricted to larger, $D_h > 5$ nm Au clusters due to the requirement for a large dilution (∼20×) of the Au nanoclusters to $\sim 5 \times 10^{-4}$ M due to their strong visible optical absorbance. DLS was used to determine D_h for the optically transparent PS column calibration standards used to calibrate the SEC columns.

D. X-ray Fluorescence (XRF). A QuantX X-ray fluorescence instrument was used to measure the Au and S concentrations and their ratio. The samples were measured in the chromatography solvent toluene using the integrated X-ray fluorescence intensity from the Au Lα and S Kα lines. We can also ascertain the absence of other impurity byproducts such as Br, Cl, or P in the purified solutions using this technique. Reference spectra with known amounts of the appropriate organometallic compounds in toluene or benzene were used to measure absolute concentrations of analytes. For example, known concentrations in the range from 10^{-4} M to 10^{-2} M of gold tri-phenyl phosphine chloride, $Au(PPh_3)_3Cl$, for Au calibration or dodecanethiol in benzene for S calibration were used. In the latter case the entire XRF chamber was purged using He to eliminate Ar interference. The samples were contained in polypropylene holders with very thin (3.6 μm) Mylar windows, and enough volume was used to ensure that all the exciting X-rays are complete absorbed (3−4 mL).

E. Synthesis. In 1978, Schmid reported that chemical reduction by gaseous diborane of a benzene solution of $Au(PPh_3)_3Cl$ (Ph = phenyl) at 50−60 °C produces a compound whose molecular weight was determined to be $Au_{55}(PPh_3)_{12}Cl_6$.[1] Experienced chemists recognize the dangers and technical difficulties associated with the use of diborane as a reducing agent and so this synthesis did not become commonplace. In addition, though the purified Au($N = 55$) clusters produced were soluble in strong solvents such as methylene chloride or pyridine, decomposition to form a mirrorlike gold coating occurred in a few days. It was hypothesized that decomposition of the tri-phenyl phosphine ligated Au($N = 55$) clusters to bare Au($N = 49$) was occurring.

We explored a modification of the Schmid approach but using less dangerous (but still pyrophoric and very air-sensitive) reductants. Such nonaqueous reductants are quite useful in the inverse micelle synthesis of metal nanoclusters and we wondered if Au($N = 55$) could be produced. The reductions were performed in an inert Ar atmosphere glovebox with continuous catalytic oxygen and water removal and detection. We prepared a stock solution of 0.01 M $Au(PPh_3)_3Cl$ in benzene and reduced this solution using a wide range of strong reductants (see Table 1) dissolved in anhydrous ethers such as tetrahydrofuran, THF. We have abbreviated these reductants with the acronyms

TABLE 1: Sample Synthesis Conditions

sample	[metal precursor]	solvent	surfactant	reductant	comment
Au_733a	$Au(PPh_3)Cl$ (0.01 M)	benzene	C12SH[a]	$LiBH_4$ (0.04 M)[b]	postsynthesis
Au_735a	$Au(PPh_3)Cl$ (0.01 M)	benzene	C12SH @1 day	LiTEBH (0.04 M)[c]	postsynthesis
Au _736a	$Au(PPh_3)Cl$ (0.01 M)	benzene	C12SH @1 day	LSAlH (0.04 M)[d]	postsynthesis
Au_465	$HAuCl_4$ (0.01 M)	octane	C12E5 (0.2 M)[e]	$LiAlH_4$ (0.04 M)[f]	
Au_465a	$HAuCl_4$ (0.01 M)	octane	+C12SH @1 h	$LiAlH_4$ (0.04 M)	postsynthesis
Au_535	HAuCl4 (0.01 M)	toluene	DDAB (5%)[i]	$NaBH_4$ (0.1 M)[h]	C6SH (0.01 M)
Au_557	HAuCl4 (0.01 M)	octane	TDAB (5%)[j]	$NaBH_4$ (0.1 M)	
Au_557a	HAuCl4 (0.01 M)	octane	TDAB (5%)	$NaBH_4$ (0.1 M)	+c12sh @1 h

[a] Dodecanethiol (0.5 M/c10). [b] Lithium borohydride (2 M/THF). [c] Lithium thexylborohydride (2 M/THF). [d] Lithium tri-ethoxyaluminohydride (0.5 M/THF). [e] Nonionic alkylated polyether with $i = 12$ hydrophobic alkyl groups, $j = 5$ ethylene ether groups (Nikko Chemicals, Japan). [f] Lithium aluminum hydride (1 M/THF). [g] Lithium tri-ethyl borohydride (1 M/THF). [h] Sodium borohydride (4.4 M/H_2O). [i] DDAB = didodecyldimethylammonium bromide. [j] TDAB = tetradodecylammonium bromide.

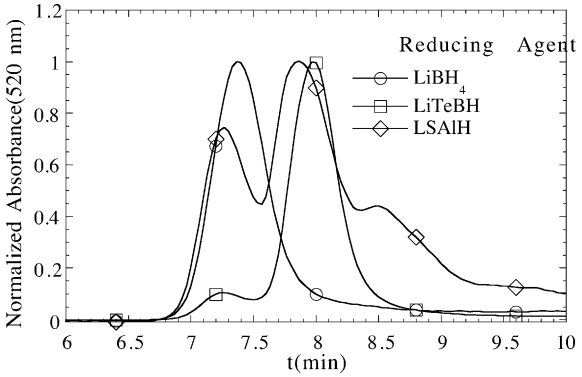

Figure 1. Normalized absorbance at 520 nm, A_n, vs elution time, t, from samples synthesized by our modified Schmid protocol. Open circles correspond to Au_733a, squares are Au_735a, and diamonds are Au_736a (see Table 1 for details).

indicated in the footnotes to Table 1, using notation identical to that in our previous papers and patent. Unless otherwise noted, all chemicals used were purchased from Aldrich, of the highest grade available, and they were opened and used as received in our glovebox.

3. Results and Discussion

Objective TEM analysis of cluster size distributions from any synthesis which produces a wide range of cluster sizes is very difficult, as the largest clusters are most easily visualized and thus tend to be weighted more strongly. The small size of the Au($N = 55$) cluster produced in the Schmid method is a good example. Published TEMs showed that larger aggregates appeared on the grid, and it was very difficult to visualize the primary, $D_c \sim 1.5$ nm clusters. If any Au($N = 13$) was present, technical difficulties would have prevented its observation.

Chemical reduction of 0.01 M $Au(PPh_3)_3Cl$/benzene in the absence of surfactants using a 2-fold excess of the various types of reductants (see Table 1) produces a wide range of cluster sizes, including metallic films which deposited over time ($\sim$1 day) on the glass. The fragility of the Au($N = 55$) species ligated with a dozen PPh_3 ligands was already noted by Schmid, so our results were not surprising.

We then added $\sim$0.01 M C12SH to these solutions and found that the metallic films actually dissolved, producing a stable solution of nanoclusters whose size distribution was studied by HRSEC with the results shown in Figure 1, identified by the type of reductant used. The alkanethiol was apparently able to etch the films and produce alkanethiol-stabilized clusters.

The effect of reducing agent and alkanethiol etchant on the elution behavior of three samples of Au clusters grown by the modified Schmid approach is shown in the SEC chromatograms of Figure 1. The amount of each size nanocluster is proportional to the absorbance amplitude and depends on the type of reducing agent used. The unnormalized peak amplitudes for the samples fall in the range of 0.1 to 0.2 cm^{-1} at 520 nm. This is within the range of the tested linear response of the detector of 0.001 to 3 cm^{-1}. The upper limit was tested by successive doubling of the volume of a sample of monodisperse Au clusters injected and verifying a doubling of the chromatogram peak area. The detector response in this figure has been normalized to that of the most abundant cluster size in each case to allow comparison of the relative amounts of each size of cluster in these polydisperse samples.

How can one determine if specific chemical interactions or size-exclusion account for the separation behavior observed in Figure 1? Three methods were used to determine if a pure SEC mechanism is operative for a given nanocluster sample. These tests are equally valid for the case of ordinary chemicals. A first test is the substitution of a zero-dead-volume coupling for the column and measurement and comparison of the cluster peak elution area to that observed with the column. An elution area ratio (column on vs no column) of between 90 and 100% was observed for all samples reported herein (i.e., all the clusters are eluting from the column to within our area measurement uncertainty). Second, if one injects increasing amounts of clusters and still observes an invariant retention time, peak shape, and a proportional increase in elution peak area, chemically specific interactions are unlikely. Finally, one examines the shape of the absorbance spectra as a function of elution time. A homogeneous shape throughout an elution peak means the peak represents a pure component or, in the case of nanoclusters which have strong size and shape dependence to their optical absorbance, a single size and shape. Specific chemical affinity effects will always increase the retention time compared to a pure SEC mechanism, leading one to infer too small a size for the molecule or cluster. For example, the tailing of the peak beyond 9 min for Au_736a (Figure 1) is due to chemical affinity since the spectra beyond t=9 min are homogeneous.

Using the calibration equation described in the Experimental Section we replot the data of Figure 1 as the hydrodynamic diameter, D_h vs normalized detector response plot in Figure 2. The detector response is approximately proportional to the cluster concentration if the molar extinction is not strongly size dependent.

Using XRF to measure the [Au] and our Cary 2300 to measure the absorbance coefficient, we find that for largest $D_c = 4.5$ nm clusters, with a well-defined absorbance peak at 516 nm, $\epsilon(520\text{ nm}) = 3200\ cm^{-1}\ mol^{-1}$, while for clusters having no absorbance peak and $D_c = 1.6$ nm, $\epsilon(520) = 2200\ cm^{-1}\ mol^{-1}$. So, the true molar abundances of the smaller clusters

TABLE 2: Size and Optical Properties of Samples

sample label	elution time (min)	column, eluant	D_h SEC	shell (nm)	D_c SEC	D_c TEM	λ_p(nm)[e]	comment
Au_733a	7.37(0.45)	PL1000/toluene	5.7	2.4	3.3	N. A.	none	majority
Au_735a	7.27(0.4)	PL1000/toluene	6.1	2.4	3.7	3.4−3.6	508	minority
Au_735a	7.97(0.4)	PL1000/toluene	3.8	2.4	1.4	1.4.−1.6	none[c]	majority
Au_736a	7.27(0.4)	PL1000/toluene	6.1	2.4	3.7	N. A.	none	minority
Au_736a	7.85(0.6)	PL1000/toluene	4.2	2.4	1.8	N. A.	none	majority
Au_736a	8.5(0.8)	PL1000/toluene	2.9	N. A.	<1.0	N. A.	none[c]	minority
Au_465	7.39(0.6)[d]	PL500/thf	3.3	2.2	1.1	N. A.	none	2 days
Au_465	6.53(0.6)	PL500/thf	5.3	2.2	3.0	2.8		30 days
Au_465a	7.04(0.35)	PL500/thf	4.0	2.2	1.8	2.0	none	2 days
Au_465a	6.84(0.40)	PL500/thf	4.5	2.2	2.3	2.2	none	30 days
Au_535	7.32(0.6)	PL1000/toluene	4.8	1.2	3.6[a]	3.5	506	2 days
Au_535	8.33(0.35)	PL1000/toluene	3.1	1.2	1.9[b]	2.0	none	2 days
Au_535	8.50(0.35)	PL1000/toluene	2.8	1.2	1.6[a]	N. A.	none	20 days
Au_535	8.90(0.4)	PL1000/toluene	2.1	1.2	0.9[b]	N. A.	none[c]	20 days
Au_557	6.16(0.6)	HR3/toluene	12.4	2.4	10	9−10	522	1 day old
Au_557a	7.87(0.35)	HR3/toluene	4.2	2.4	1.8	2.0	none	+C12SH

[a] Minority or shoulder on SEC size distribution. [b] Majority peak. [c] Discrete molecular electronic transitions observed. [d] Line width (fwhm) of 99.5% c60 (Strem Chemicals) is 0.42 min on this column. [e] λ_p = peak absorbance wavelength.

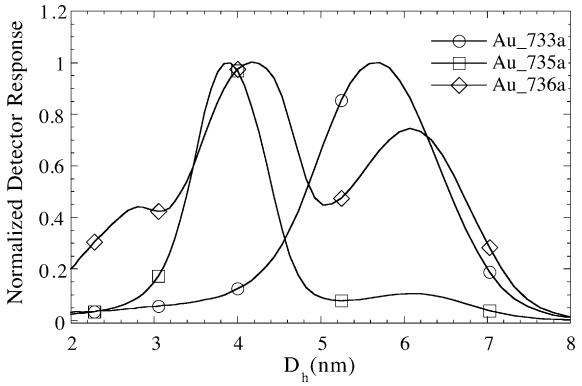

Figure 2. Normalized detector response from the cluster absorbance at 520 nm vs D_h for samples synthesized by a modified Schmid protocol. Open circles label the chromatogram for sample Au_733a, squares are Au_735a, and diamonds are Au_736a (see Table 1 for details).

are larger than the normalized detector response shown in this figure by about 50%.

We can calculate the average inorganic core size from D_h in Figure 2 by subtraction of the shell thickness due to the alkanethiol on the metal cluster surface where, for dodecanethiol, a total thickness 2.4 ± 0.1 nm was previously determined.[2] This total thickness is less than that of the fully extended chain length, but is very similiar to that found by elliposometric measurement of Au ⟨1,1,1⟩ films with an adsorbed monolayer of dodecanethiol where 1.1 nm was found for extended 2-D films. This would predict a 2.2 nm shell thickness for a spherical nanoparticle—close to that observed by us.[18]

To determine the thickness of the organic shell as a function of alkyl chain length, a monodisperse sample was grown in a nonionic surfactant micelle. Its core size was determined by TEM to be 1.9 ± 0.2 nm. The sample was subsequently subdivided and different chain length alkanethiols ranging in length from 8 to 18 carbon atoms were added to each daughter sample and SEC elution peak times were obtained. A best fit to a $\log(D_c + \text{thickness})$ vs t yields the best thickness estimate for that particular core size.

We have found this thickness is slightly dependent on the core size, contracting with increasing core size as the hydrophobic alkyl chains lay down on the metal surface for core sizes greater than ∼4−5 nm. However, in the present work we will assume it to be core-size invariant, since this contraction effect is only a few angstroms. Though we can determine both the peak retention time and thus D_h with a precision of three significant figures for a given sample, we only report D_c to two figures in Table 2 due to the organic shell thickness uncertainty combined with the measurement uncertainty (∼±10%) inherent in TEM core-size determination of ∼2 nm clusters.

Subtraction of a constant total shell thickness of 2.4 nm shows that for the trimodal Au_736a sample there are peaks at $t =$ 7.2−7.3 min ($D_c \sim 6$ nm), 7.8−8.0 min ($D_c = 1.6-1.8$ nm), and $t \sim 8.3-8.5$ min ($D_c \sim 0.5-1.0$ nm) in one or more of the samples shown in Figure 2 (see also Table 1). We have previously demonstrated[6] that the strength of the reductant influences the size of the final clusters in the case of the inverse micelle method-stronger agents (e.g., $LiAlH_4$ vs $LiBH_4$), producing smaller nanoclusters, and this trend seems to hold here too, with lithium tri-ethoxyaluminohydride (LSAlH) producing a larger number of clusters smaller than 1 nm.

In Figures 1 and 2, the elution peak at $t = 8.5$ min, $D_c \sim$ 0.5−1.0 nm, corresponds closely to ∼1 complete shell or $N \sim$ 13 atoms of Au, the peak at $t = 8.0$ min with $D_c = 1.4-1.6$ nm corresponds to two completed atomic shells or $N = 55$, the majority product in the original Schmid synthesis. In the case of the synthesis using lithium thexylborohydride (LiTEBH), this appears to be the most abundant product. Furthermore, unlike the PPh_3 ligated Au($N = 55$) clusters of the original Schmid synthesis, the strong alkanethiol−Au ligation makes such clusters very stable long term in solution. By contrast, Au cluster samples synthesized without the addition of alkanethiols either during or after the synthesis fail to elute since the tri-phosphine ligand is completely separated from the clusters by the SEC column and PPh3 can be detected quantitatively using the RI detector.

The other elution peaks observed in Figure 2 correspond to 3 shells or $D_c = 1.8-2$ nm ($N \sim 147$), $t = 7.4$ min, $D_c = 3.3$ nm (5 shells, $N \sim 560$), and $t = 7.3$ min, $D_c = 3.7$ nm (6 shells, N ∼ 920 atoms). The latter two populations show up frequently as well-ordered regions in TEM images of these Au clusters samples—demonstrating the possible misleading nature of TEM size analysis (see supplementary Figure 2S).

How does this size evaluation by SEC compare to TEM images of these polydisperse samples? Since the largest clusters in each sample tend to size segregate and form ordered arrays, as shown in Figure 3 taken at a magnification of 100K×, at 120 keV, ordered regions of 3.4−3.6 nm particles appear to represent the majority of particles, but there are also dispersed

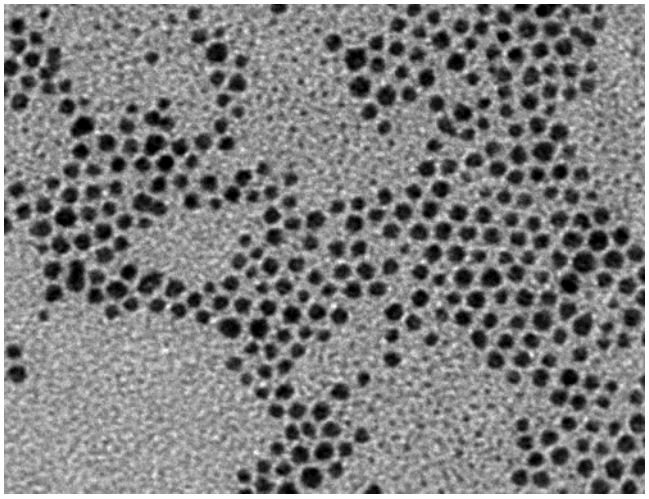

Figure 3. TEM of sample Au_735a taken at 100K× , 120 keV. Ordered regions with particles in the 3−4 nm range appear to be the majority but lower contrast $d = 1.6$ nm particles can also be seen in this region.

∼1.4−1.6 nm particles present in what appears to be smaller numbers. By contrast, Figure 2 demonstrates that the peak at $D_c = 4$ nm − 2.4 nm = 1.6 nm represents the majority population, while the small peak at $D_c = 6.1 - 2.4 = 3.7$ nm is the minority population. So, although there is good agreement between the mean core sizes for these two populations observed by both techniques, SEC shows that the 1.6 nm core size particles are especially favored by the thiol etching process.

The large spread in size observed in both the SEC and TEM data of Figures 2 and 3 shows that, although special closed shell sizes may be favored during the etching process, a wide range of possible cluster sizes are produced. However, the prevalence of certain sizes is obvious and the question is what may account for this observation?

As Schmid has pointed out,[17] metal clusters ligated by bulky groups may restructure to form a highly symmetrical ligand envelope consistent with a closed shell of metal atoms. The larger facets will provide the necessary surface area for attachment of relatively bulky organic ligands. In analogy to extended metal surfaces, the ligands cause a reconstruction of the metal cluster geometry to lower the total energy of the clusters. This can actually result in a reduced density for the inorganic core compared to bare spherical clusters with cubic close packing, such as are produced by supersonic expansion of atoms into a vacuum. In this solution etching process the thiols seem to favor certain sizes.

Our results show that the relative abundance and average cluster size in this modified Schmid synthesis depends not only on the type of reductant but also on the details of the etching process due to the post-reduction addition of dodecanethiol. As noted by others,[10] alkanethiols in neat form at elevated temperatures can etch and partially dissolve Au nanoclusters. What is surprising is the efficacy of this etching effect under these dilute, ambient conditions on the metallic cluster films deposited onto the glass of our reaction vial. We speculate that our metallic films are similar to the decomposition product of $Au_{55}(PPh_3)_{12}Cl_6$ first noted by Schmid. Recent observations on the sintering of alkylthiol-ligated Au and Pt nanoclusters give some insight into the possible microstructure of these films.[18]

It is worth noting that strong evidence for limited etching of extended 2-D Au ⟨1,1,1⟩ surfaces has been reported in the literature. This etching was invoked to explain the holes or pits formed in Au−thiolate monolayer films as observed in STM or AFM images. The presence of Au in the deposition solutions used to form the thiolate monolayers was posited to occur due to removal of a single layer of Au atoms via formation of a Au−thiolate complex in selected holes or pits of the film.[20,21]

Our modified synthesis can produce large amounts of Au−thiolate complexes with a core size corresponding to $Au_{55}(PPh_3)_{12}$ as first described by Schmid which was shown to have a 4:1 or 5:1 Au/ligand ratio. However, most elemental analysis[9] of the Au/S ratio of Au−alkanethiolate clusters powders purified by chemical precipitation have determined values of around 2−2.5:1 for the Au/S ratio. We have performed X-ray fluorescence elemental analysis on SEC-purified toluene solutions of Au/dodecanethiol samples with $D_c \sim 1.6-1.8$ nm and found a value of around 5:1. This is consistent with the structural model of Schmid.[17] Even solutions purified by chemical precipitation by methanol and redissolved in toluene show values of at least 4:1.

XRF elemental analysis of nanoclusters has the advantage that the sample can be studied in situ in the solvent, toluene, and directly compared to Au and S elemental standards also in toluene or xylene. This improves the absolute determination of the metal concentration since matrix and preparation effects inherent to alternative analytical methods are eliminated. However, the unfortunate energy overlap of the Au Mα and S Kα XRF lines means that the Au Mα line peak area must be subtracted from the total Au + S XRF signal rather than deconvoluted from the S Kα line. So our uncertainty is larger (∼20%) than we would like. However, purification by SEC is probably better than chemical precipitation and washing methods, which typically require some free thiol be present in the nonsolvent to avoid irreversible cluster aggregation. This free thiol, if partially coprecipitated with the nanoclusters, could boost the apparent [S] in the analyzed powder precipitate.

What are the size-dependent optical absorbance properties of the various subpopulations of Figure 2? Since we obtain absorbance spectra every 2 s (∼2 Å size resolution at an mobile phase flow rate of 1 mL/min) throughout the experiment, this information is readily available. The elution time-dependent spectra confirm and extend to molecular sizes our recent SEC observations of the size-dependent properties of monodisperse, inverse micelle synthesized Au and Ag clusters[13] as well as those reported in our first publication on the optical properties of colloidal gold.[6]

In Figure 3 we show the spectra for the $D_c \sim 1$, 1.6−1.8, and 3.7 nm Au cluster subpopulations at the peak apex positions of the chromatogram of sample Au_736a of Figure 1. The strong damping, blue-shift, and increased absorbance in the NIR and NUV regions of the spectra with decreasing size has been described by us and others.[13,22−24] In the case of the clusters whose size is less than 1 nm, distinct, nonclassical (i.e., molecular) absorbance features are observed in room-temperature data. Whetten's research group has reported such discrete features in a 9 kD Au cluster which has nonclassical features such as near-IR photoluminesence (PL) analogous to the visible PL we first reported for Au clusters etched in aqueous solution.[25−27]

The data of Figure 4 are consistent with the retention time (i.e., hydrodyamic size) and absorbance spectra previously reported for nearly monodisperse samples of Au synthesized in inverse micelles,[13] which establishes that a SEC mechanism, not chemical affinity of the clusters for the column, is separating the clusters.

The good size selection capability of HRSEC allows one to observe new absorbance features in the $D_c \sim 1$ nm, $N \sim 13$

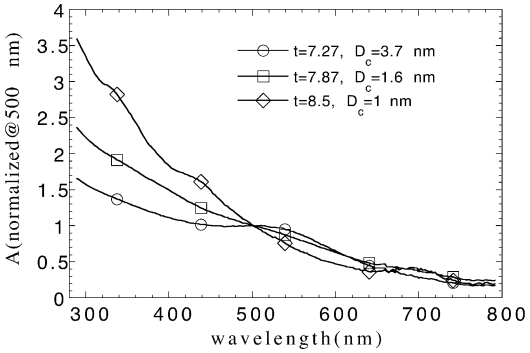

Figure 4. Plot of peak elution spectra (elution times are indicated) vs wavelength. A distinct absorbance onset near 700 nm or 1.75 eV (the interband transition) is observed in the smallest cluster sub-populations. Open circles label the $D_c = 3.7$ nm peak, squares the $D_c = 1.6$ nm peak, and diamonds the $D_c \sim 1$ nm peak spectra.

subpopulation without resort to differentiating the absorbance spectrum. The larger $D_c \sim 1.6-1.8$ nm, $N \sim 55$ atom cluster has the familiar lack of features first reported by Schmid and Kreibig[28] for purified $Au_{55}(PPh_3)_{12}$ clusters and reported by Whetten et al. for their ubiquitous 29 kD fraction ($D_c \sim 1.6-1.7$ nm) made using an inverse micelle synthesis in the presence of thiols as etchants. This 29 kD fraction was identified using MALDI TOF mass spectroscopy.

Our $D_c \sim 1.6-1.8$ nm sub-population has significantly more absorbance at high energies than our larger $D_c \sim 3.7-4.0$ nm, $N \sim 1000$ fraction whose spectra exhibit a red-shifted absorbance maximum at 508 nm. This resonance still has considerably more damping than expected from Au colloids with $D_c \sim 10$ nm which have an expected plasmon at 520−530 nm in toluene and can be adequately described by classical Mie theory.

What relationship do the present spectra for the very small $D_c < 1.0$ nm, $D_c \sim 1.2-1.4$ nm, and $D_c \sim 1.6-1.8$ subfractions have to previously observed spectra of small gold clusters? In supplementary Figure 1s, we have coplotted data from ref 26 with our spectrum from the $t = 8.5$ min, $D_c < 1$ nm, subpopulation of sample Au_736a. A typical TEM region of this sample is shown in supplementary Figure 3s. The data for Whetten's well-characterized Au/glutathione, $N = 28$ sample in water resembles our smallest $t = 8.5$, $D_c < 1.0$ nm, $N = 13$ fraction in the blue-UV region, with much stronger absorbance compared to our larger, $t = 7.9$, $D_c \sim 1.6-1.8$, $N \sim 150$ fraction or the SEC-purified putative 8 kD Au/thiolate, $D_c \sim 0.9$ nm spectra from ref 10. Both of the thiol-etched fractions from refs 10 and 23 have stronger NIR absorbance than our fractions. However, our smallest fraction has similar molecular features in the visible region.

One possible source of differences in the present sample from previous work arises from an assumption of cubic packing in estimating the size from the measured molecular weight in ref 23. If cubicosahedral packing were assumed, for the same number of atoms, the 9 kD Au clusters would be larger, $D_c \sim 1.2$ nm. Another difference is the solvent phases, water and toluene, respectively, and the ligands, glutathione, and dodecanethiol. It would be surprising if such interfacial differences did not effect the d interband energy levels of such small Au clusters. In any case, the distinct nonclassical features observed in both the Au/glutathione, $N = 28$ Au molecule and our $D_c < 1.0$ nm, $N \sim 13$ Au fraction are common to both samples, though the two synthetic approaches are quite different.

This etching process is obviously extremely complex in such strongly polydisperse samples. It can be simpler in the case of quasi-monodisperse samples prepared by inverse micelle methods as we show in the next part of this paper.

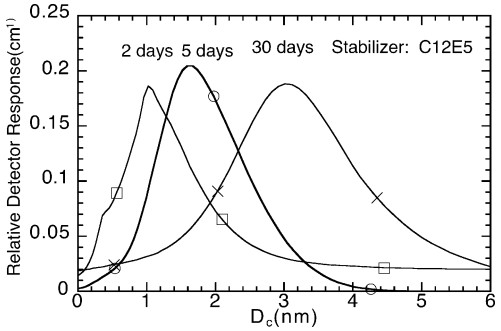

Figure 5. Relative numbers of particles as monitored by the cluster absorbance at 520 nm vs core size D_c obtained from the elution time. The sample is Au_465, the column is a PL500 type, the mobile phase is THF. Open squares label the curve for 2 days, open circles for 5 days, and crosses the curve for 30 days.

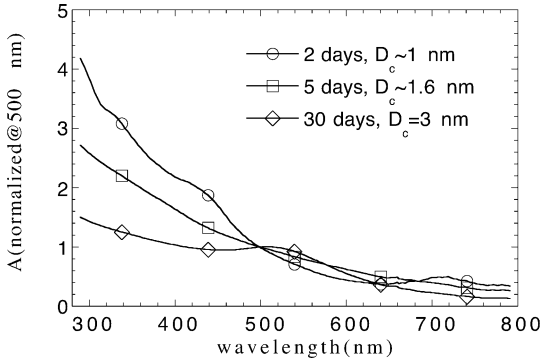

Figure 6. The peak apex spectra for the absorbance chromatograms of Figure 5 are shown, normalized to 500 nm to allow a comparison of the shape. Open circles represent a 2 day old sample, squares represent 5 days, and diamonds represent 30 days.

4. Aging and Etching during Inverse Micelle Synthesis

A. Aging. Due to facile cluster diffusion in liquids and intercluster atomic exchange processes, time-dependent changes may occur in a cluster size distribution. This topic remains largely unexplored due to the paucity of rapid feed-back techniques for objective size-distribution analysis of nanoclusters. Changes at the cluster surface which depend on the chemical nature of the reductant (i.e., $LiAlH_4$ vs $LiBH_4$) can also affect the SEC behavior since nanocluster surface interaction with a given type of column material can lead to peak tailing just as is commonly observed in surfactant systems.

As we now show in this paper for the case of nanosize gold, and have recently observed for nanosized semiconductors,[3] structural annealing or aging in nanocluster solutions often occurs spontaneously under ambient conditions. The observed changes in the average cluster size, surface morphology or chemistry, and optical properties are readily monitored by SEC, though their interpretation is nontrivial. These surface chemical and/or structural changes depend on the type of surfactant(s) used in the synthesis and even on the hydrophobicity of the solvent.

Figure 5 shows the raw, convoluted size distribution obtained by using a PL500 column and THF as the mobile phase to analyze sample Au_465 (see Tables 1 and 2 for synthetic, size details) as a function of age. The average cluster size increases with time, as further supported by a red-shift of the absorbance peak with age, shown in Figure 6. The mean sizes shown are

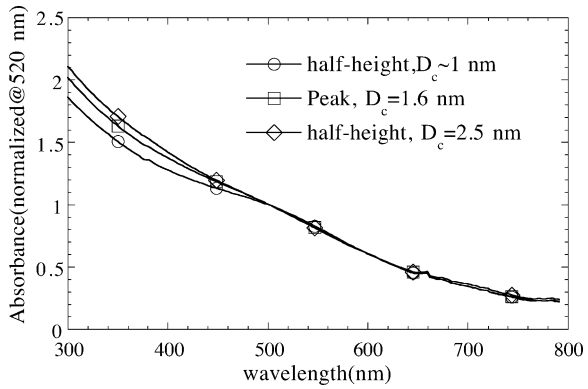

Figure 7. The spectral homogeneity within the elution peak corresponding to Au_465 aged for 5 days (Figure 5) normalized at a common wavelength, 520 nm, is very good, demonstrating homogeneity of cluster size and shape. The open circles correspond to the half width at half-height (HWHH) spectrum, the squares to the peak apex spectrum, and the diamonds to the other HWHH spectrum.

1, 1.6, and 3 nm, which correspond closely to those observed as the most abundant populations in the modified Schmid synthesis.

The spectra of Figure 6 also correspond closely to the corresponding spectra of the three subpopulations of sample Au_736a whose spectra was shown in Figure 4, with nonclassical structure observed for the $D_c \sim 1$ nm population, a loss of all features for the $D_c \sim 1.6$ which corresponds closely to the $N = 55$ closed shell size, and the $D_c = 3.0$ nm spectrum which actually shows an absorbance maximum at 504 ± 4 nm.

There is a slight increase in the polydispersity of the samples with age, though a significant amount of the apparent size dispersity shown in Figure 5 is due to the instrumental broadening since the spectra within a given peak are very homogeneous in shape as shown in Figure 7 for the sample aged for 5 days. The absorbance of Au clusters is known to be very sensitive to both size and shape, as demonstrated in Figure 6, so spectral homogeneity requires size and shape homogeneity throughout an elution peak.

If no instrumental broadening occurred, then one would expect the spectrum of the $t = 5$ days sample at the half width at half-height location in the chromatogram of Figure 5 which corresponds to $D_c \sim 1$ nm to be identical in shape to that of the peak apex spectra of the sample aged for 2 days. This is not the case (see Figure 7).

The reader can examine supplementary Figure 3s to confirm that the average core size from TEM of sample Au_465 aged for 30 days is ~3.4 nm with significant polydispersity (~±0.5 nm), consistent with increased width of the corresponding chromatogram in Figure 5.

Sample Au_465a with dodecanethiol added immediately after the reaction shows much slower changes in average size with time (Figure 8). The mean size at $t = 2$ days is 1.8 nm with a range of sizes from 1.4 to 2.1 nm (HWHH) while the mean size at $t = 30$ days is 2.1 nm with a range in sizes of, at most, 1.6 to 2.7 nm. These size dispersions overestimate the true polydispersity since the instrumental response adds to the apparent line width.

Chemical changes may also occur at the surface of freshly synthesized clusters. In fact, clusters studied within a few hours of synthesis often show poor peak symmetry and incomplete elution. The slight asymmetry in the $t = 2$ day elution profile shown in Figure 8 and the significantly lower amount of clusters which elute are due to residual chemical interaction between the freshly synthesized clusters and the column which leads to

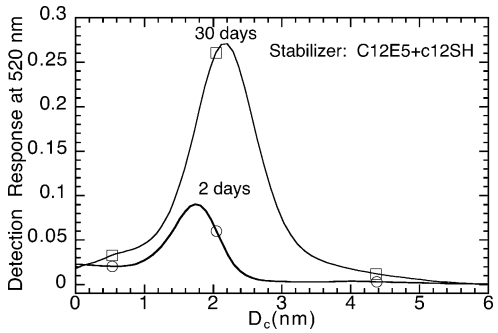

Figure 8. Detector absorbance at 520 nm vs core size D_c obtained from the elution time. The sample is Au _465a, the column is a PL500 type, the mobile phase is THF. Curve labled with circles is $t = 2$ days, while the curve with squares corresponds to $t = 30$ days.

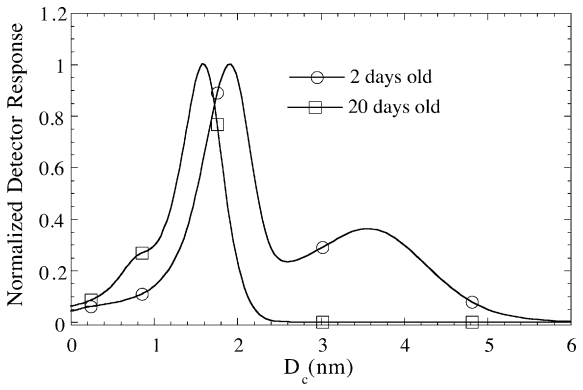

Figure 9. Effect of aging and etching by hexanethiol of sample Au _535. The open circles represent 2 days of aging, while the open squares correspond to 20 days.

peak tailing at longer times (smaller apparent sizes). The absorbance spectra are quite homogeneous throughout both of the peaks.

These aging phenomena are ubiquitous in many types of nanoclusters and may be due to the effectively lower melting transition of clusters. Clusters with greater than 50% of all atoms in surface sites have significant numbers of highly mobile atoms whose cooperative movement permits facile defect diffusion and changes in surface structure as well as intercluster atomic exchange upon collisions with other clusters.

It is interesting to note that similar reconstruction of 2-D Au-⟨1,1,1⟩ surface films appears to occur in the presence of monolayers of alkanethiols. STM measurements at low tunneling currents, ~1 pA, where imaging artifacts are absent show edge migration and movements of holes at step terrace boundaries in the films due to the high surface mobility of the Au atoms bound to the thiols.[18,21] Lateral force AFM measurements confirm these observations.[29] Au−thiolate complexes appear to readily detach from the surface and then migrate to new locations. In the present experiments collisions between clusters in solution appear to allow exchange of Au atoms, possibly via an analogous Au−thiolate complex.

B. Etching Effects. Addition of even dilute amounts of alkanethiols to solutions of Au nanoclusters can lead to a redistribution of cluster mass via etching. Our experiments indicate that the rate of etching increases with decreasing alkyl chain length. (The limiting case, H_2S, is a major etchant of even bulk metals such as brass regulator valves!) Figure 9 illustrates the etching which occurs in sample Au_535 (see Tables 1 and 2) in the presence of hexanethiol where, over a period of 2 weeks, a complete loss of the minority larger $D_c = 3.6$ nm (~6 shells, $N \sim 920$ atoms) population occurs, together with a loss

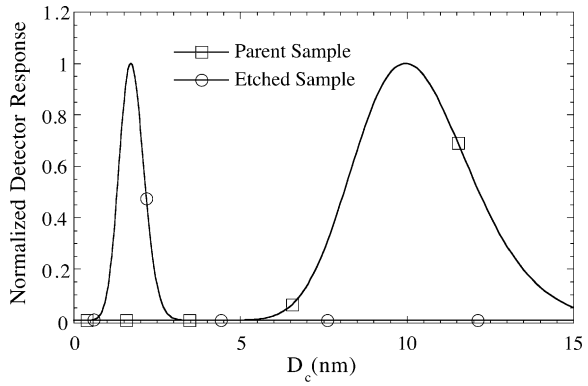

Figure 10. Effect of etching of sample Au_557 after addition of dilute dedecanethiol and a time period of less than 1 day under ambient conditions in toluene. The curve labeled with open squares is the initial population, while the curve with open circles is the sample 1 day after addition of the thiol.

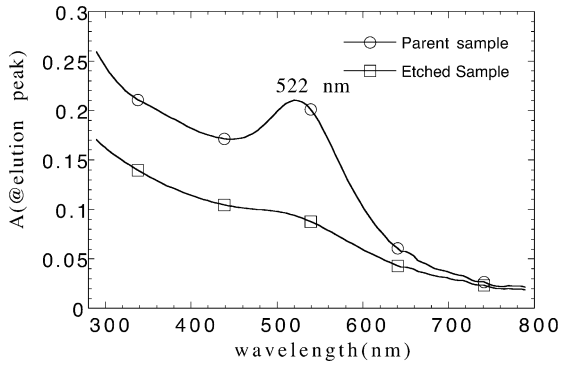

Figure 11. Absorbance spectra of sample Au_557 at the peak apex of elution of Figure 10 illustrates the blue-shift and disappearance of the plasmon with etching to a smaller size. Open symbols label the parent sample absorbance, while open squares label the absorbance data after the etching occurs.

of the majority population at $D_c = 1.9-2.0$ (3 shells or $N = 147$ atoms). Mass redistribution of atoms into a majority cluster population with $D_c = 1.6$ nm ($\sim$2 shells or $N = 55$ atoms) and a small shoulder at $D_c \sim 0.9$ nm ($\sim$1 shell, or $N \sim 13$ atoms) occurs. These critical sizes (retention times) are commonly observed as seen from Table 2. As in our modified Schmid synthesis, the optical absorbance corresponding to the smaller etched population with a core size between 1.5 and 1.6 nm exhibits a broad dispersion or width, while the smallest etched clusters with $D_c \sim 1$ nm show nonclassical structure in their absorbance.

Over an identical period of time a monodisperse sample made using the longer chain dodecanethiol and also stored in toluene under ambient conditions gave SEC elution at $t = 7.37$ min, $D_c = 3.8$ nm, and its size distribution (line width) and optical behavior were invariant. (See Supporting Information, Figure 4s.)

Etching is minimized in very hydrophobic solvents such as hexadecane and occurs more readily in the presence of cationic surfactants such as didodecyldimethylammonium bromide or tetradodecylammonium bromide compared to nonionic surfactants such as pentaethylene gylcol *n*-dodecyl ether, c12e5.

Figure 10 illustrates the dramatic etching which occurs in less than 24 h upon introduction of only 0.01 M dodecanethiol into and 0.01 M sample Au_557 synthesized in the two-component inverse micelle tetradodecylammonium bromide/toluene. The initially red solution changes to orange in color as it etches. The plasmon maximum at $\lambda_p = 522$ nm from the $D_c \sim 10$ nm clusters broadens and disappears with the etching process as shown in Figure 11.

In previous work on alkanethiolate monolayers on Au(111) it was found that shorter chain thiols at higher concentrations resulted in substantially more observed Au in the methanol solutions used to deposit the thiolate films. This was attributed to the larger solubility of Au(I)−thiolate species in the relatively polar solvent methanol.[29] However, less Au was detected by atom absorbance spectroscopy than would be expected by the pit or hole density observed by STM in the films, so some redeposition or restructuring without loss of Au must have been occurring in these experiments as well. It would be very interesting to repeat these experiments using the nonpolar deposition solvents such as were used in the present studies to see if a reduced amount of etching occurred.

We find that once the ratio of thiol/Au exceeds 1:1 no further etching or size change occurs in the nanoclusters. It appears that, as in the case of Au−thiolate films, the etching process proceeds only until a stable final structure is achieved.[21] In our case, this final structure appears to be close to the thermodynamically stable closed atomic-shell size. In the case of films, only a single layer of Au seems to be removed in the 3−5 nm holes or pits observed in STM, so again the etching process is completed once the thiolate film achieves an optimal packing over the entire surface. The Au removed to form these pits or holes in the Au⟨1,1,1⟩ layer might actually be in the form of Au−thiolate clusters of a thermodynamically stable size.

5. Conclusions

We have demonstrated a modified, surfactant-free synthesis of Au nanoclusters based upon the method of Schmid. Such nanocluster samples exhibit a wide range of sizes and even metallic film formation with age. Addition of dilute amounts of the alkanethiols such as dodecanethiol etches away the metallic film, and HRSEC reveals that certain prevalent sizes are formed which correspond closely to that predicted by the cubicosahedral packing of metal atoms into closed shells. Thus, cluster structural stability may determine the final cluster size distribution in a size regime less than 4 nm.

The Au($N = 55$) species first observed by Schmid is found in large abundance with a properly chosen anhydrous reductant. The chemical nature of these reductants strongly influences the relative amounts of the subpopulations which are produced in our modified Schmid synthesis. We can produce large amounts of a molecular sized species with $D_c < 1$ nm which likely corresponds to the first closed shell icosahedra with $N \sim 13$ atoms, using the strongest reductants such as lithium triethoxyaluminohydride. HRSEC PDA optical spectra for size-selected subpopulations show the absorbance features that may be associated with discrete interband transitions in Au nanoclusters. A comparison to the absorbance of an 8 kDa Au/glutathione cluster in aqueous solution[26] shows very similar features.

Both TEM and HRSEC demonstrate that in the modified Schmid synthetic protocol, certain cluster sizes are observed which are very close to that expected for closed icosahedral shells of atoms. Nearly every closed shell size up to $N = 5$ shells was observed in these populations. However, significant size dispersion around these special sizes was also observed.

We next explored the role of alkanethiols as chemical etchants during metal cluster synthesis in inverse micelles. We demonstrated that the rate of etching depends on the length of the alkyl chain, just as it does for Au⟨111⟩ films. For hexanethiol, etching is rapid in solvents such as toluene, and decreases as

the thiol alkyl chain length increases. The etching process was shown to produce clusters whose sizes approximated closed shell atomic configurations. An interesting observation was that etching could be strongly suppressed in very hydrophobic solvents such as hexadecane.

The extremely precise and rapid size and optical analysis capabilities of HRSEC allowed us to investigate, for the first time, the time evolution of the cluster size distribution of nanocluster samples synthesized in inverse micelles. In the case of nonionic alkylated polyether surfactant micelles, an increase in size with age was typically observed from $D_c \sim 1.1$ nm to $D_c \sim 3.0$ nm over a period of 30 days or less. In the presence of dodecanethiol added post-reduction to these solutions, an etching and narrowing of the cluster size distribution occurred over a similar time span, the final size having close to 3 closed shells or ~147 atoms. This verifies the size narrowing observed in ref 10 during etching with neat thiols at elevated temperature, but in our case occurs under ambient conditions with dilute thiol solutions.

Acknowledgment. This work was supported by the Division of Materials Science and Engineering, Office of Science, U.S. Department of Energy under contract DE-AC04-AL8500. Sandia is a multiprogram laboratory operated by Sandia Corporation, a Lockheed-Martin Company, for the U.S. Department of Energy.

Supporting Information Available: Electron micrographs of selected samples whose HRSEC is shown are used to illustrate some of the shortcomings of TEM analysis of size distribution. A comparison of the size-dependent optical spectra from refs 26 with the present extremely small Au nanocluster sub-populations is also shown. This material is available free of charge via the Internet at http://pubs.acs.org.

References and Notes

(1) Schmid, G. *Angew. Chem.* **1978**, *90*, 417.

(2) Wilcoxon, J. P.; Martin, J. E.; Provencio, P. *Langmuir* **2000**, *16*, 9912.

(3) Wilcoxon, J. P.; Provencio, P. *Proceedings of the SPIE on conference on "Optical Properties of Nanocrystals"*, Seattle, WA, July 7−11, 2002.

(4) Wilcoxon, J. P.; Williamson, R. L. *Proceedings of the MRS* 1989, Boston, MA.

(5) Wilcoxon, J. P. U.S. Patent 5,147,841, issued Sep. 15, 1992.

(6) Wilcoxon, J. P.; Williamson, R. L.; Baughman, R. J. *J. Chem. Phys.* **1993**, *98*, 9933.

(7) Brust, M.; Walker, D.; Bethell, D.; Schiffrin, D. J.; Whyman, R. J. *Chem. Soc., Chem. Commun.* **1994**, 801.

(8) Whetten, R. L.; Khoury, J. T.; Alvarez, M. M.; Murthy, S.; Vezmar, I.; Wang, Z. L.; Stephen, P. W.; Clevelenad, C. L.; Luedtke, W. D.; Landman, U. *Adv. Mater.* **1996**, *8*, 428.

(9) Schaaff, T. G.; Shafigullin, M. N.; Khoury, J. T.; Vezmar, I.; Whetten, R. L. *J. Phys. Chem. B* **2001**, *105*, 8785.

(10) Schaaff, T. G.; Whetten, R. L. *J. Phys. Chem. B* **1999**, *103*, 9394.

(11) Lin, X. M.; Sorensen, C. M.; Klabunde, K. J. *J. Nanoparticle Res.* **2000**, *2*, 157.

(12) Wilcoxon, J. P.; Craft, S. A. *NanoStructured Mater.* **1997**, *9*, 85.

(13) Wilcoxon, J. P.; Martin, J. E.; Provencio, P. *J. Chem. Phys.* **2001**, *115*, 998.

(14) Yau, W. W.; Kirkland, J. J.; Bly, D. D. In *Modern Size-Exclusion Liquid Chromatography*; Wiley-Interscience: New York, 1979.

(15) Martin, J. E.; Wilcoxon, J. P.; Odinek, J.; Provencio, P. *J. Phys. Chem. B* **2000**, *40*, 9475.

(16) Martin, J. E.; Wilcoxon, J. P.; Odinek, J.; Provencio, P. *J. Phys. Chem. B* **2002**, *106*, 971.

(17) Schmid, G. *Structure and Bonding*, 62; Springer-Verlag: Berlin, 1985; pp 52−82.

(18) Chaijapukui, O.; Sun, L.; Xu, C.; Crooks, R. M. *J. Am. Chem. Soc.* **1993**, *115*, 12459.

(19) Martin, J. E.; Odinek, J.; Wilcoxon, J. P.; Anderson, R. A.; Provencio, P. *J. Phys. Chem. B* **2003**, *107*, 430−434.

(20) Schonenberger, C.; Sondag-Huethorst, J. A. M.; Jorritsma, J.; Fokkink, L. G. J. *Langmuir* **1994**, *10*, 611.

(21) Sondag-Huethorst, J. A. M.; Schonenberger, C.; Fokkink, L. G. J. *J. Phys. Chem.* **1994**, *98*, 6826.

(22) Fauth, K.; Kreibig, U.; Schmid, G. *Z. Phys. D* **1991**, *20*, 297.

(23) Schaaff, T. G.; Shafigullin, M. N.; Khoury, J. T.; Vezmar, I.; Whetten, R. L.; Cullen, W. G.; First, P. N.; Gutierrex-Wing, C.; Ascnsio, J.; Jose-Yacaman, M. J. *J. Phys. Chem. B* **1997**, *101*, 7885.

(24) Alvarez, M. M.; Khoury, J. T.; Schaaff, T. G.; Shafigullin, M. N.; Vezmar, I.; Whetten, R. L. *J. Phys. Chem. B* **1997**, *101*, 3706.

(25) Bigioni, T. P.; Whetten, R. L.; Dag, O. *J. Phys. Chem. B* **2000**, *104*, 6983.

(26) Link, S.; Beeby, A.; FitzGerald, S.; El-Sayed, M. A.; Schaaff, T. G.; Whetten, R. L. *J. Phys. Chem. B* **2002**, *106*, 3410.

(27) Wilcoxon, J. P.; Martin, J. E.; Parsapour, F.; Wiedenman, B.; Kelley, D. F. *J. Chem. Phys.* **1998**, *108*, 9137.

(28) Fauth, K.; Kreibig, U.; Schmid, G. *Z. Phys. D* **1989**, *12*, 515.

(29) McDermott, C. A.; McDermott, M. T.; Green, J. B.; Porter, M. D. *J. Phys. Chem.* **1995**, *99*, 13257.